Uncertainty of the Critical Venturi Transfer Standard Used in the K6 Gas Flow Key Comparison

John D. Wright, National Institute of Standards and Technology

Abstract
The uncertainty of a critical flow venturi (CFV) gas flow transfer standard with dedicated, redundant pressure and temperature instrumentation is analyzed. At lower flows (≈5 g/min), the standard uncertainty of the transfer standard was 0.026 %. At higher flows (≈200 g/min), the standard uncertainty was 0.019 %. The largest uncertainty components were: 1) environmental temperature effects, 2) pressure sensors, and 3) the critical flow function. Temperature effects for the CFV transfer standard resulted from: 1) temperature sampling errors, 2) thermal boundary layers, and 3) thermal expansion of the CFV throat. Temperature effects on small CFVs were more significant than for large CFVs.

Introduction
Critical flow venturis (CFVs) are generally accepted as the most appropriate transfer standard in comparisons of gas flows greater than 1 L/min.[1] The transfer standard (TS) for a recent low-pressure gas flow key comparison (CCM.FF-K6) comprised of a set of eight critical flow venturis (CFVs) with dedicated pressure and temperature instrumentation (see Figure 1). Most participants tested the TS with two CFVs in series. The TS had redundant sensors for measuring the CFV pressures and temperatures (2 upstream CFV pressures and temperatures, 2 downstream pressures and temperatures). The redundant pressure, temperature, and flow measurements allowed us to assess the TS calibration stability throughout the comparison.

The advantages of CFVs include:
Mechanically Robust: CFV throat diameter is stable during normal usage and the discharge coefficient is weakly sensitive to changes in the surface finish due to dust or scratches. The CFVs themselves are essentially immune to shock. However, pressure and temperature sensors are not. Hence, the stability of the discharge coefficient is limited by the stability of the temperature and pressure instrumentation used.
Established Physical Model: The physics governing CFV behavior is well developed and experimentally verified so the influence of flow, gas composition, and first order temperature effects can be accurately predicted.
Installation Effects: Compared to most other flowmeter types, CFVs are weakly sensitive to errors due to distorted velocity profiles. By following the ISO-recommended[2] ratio of approach–to-throat diameters (4 to 1) and shipping inlet and outlet tubes with the transfer standard, installation effects are negligible.

Before starting the key comparison, we evaluated the transfer standard at NIST to assess the influence of inlet gas temperature and room temperature on the CFV discharge coefficients. We also studied the flow errors introduced by differences in the pressure ratio across the CFV. Such sensitivities in the TS will appear as lab to lab differences and therefore should be corrected if possible, or limited in magnitude and included in the uncertainty analysis of the comparison. The results of the preliminary experiments were

used to establish the temperature and pressure requirements for using the TS as well as the uncertainty introduced by the TS in the comparison results even when the TS was operated within the condition requirements of the protocol.

This paper presents results from the preliminary TS evaluation, describes how these evaluations were used to establish the operating conditions required by the protocol, and gives an analysis of the uncertainty introduced by the TS into the comparison results.

Description of the Transfer Standard

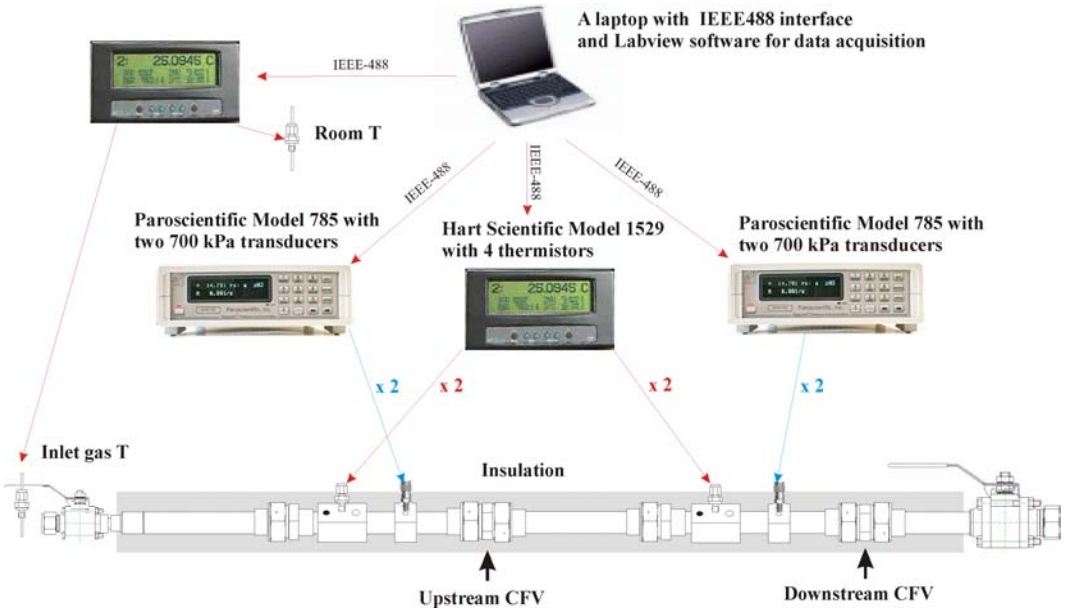

Figure 1. A schematic of the transfer standard. Room and inlet gas temperatures are monitored and the TS is insulated to control temperature sensitivities.*

The 8 CFVs in the transfer standard are normally tested as 4 pairs called Small A, Small B, Large A, and Large B. (See Figure 2.) The pairs called Small A and Small B are nominally the same and are tested on different occasions. The same is true for the pairs called Large A and Large B. A lab that is able to perform all of the measurements in the test sequence makes 140 individual flow measurements (2 CFV sets × 7 flow set points × 5 repeats × 2 occasions). K6 compared *mass flow* measurements from each lab using the discharge coefficient, C_d, for the eight CFVs:

$$C_d = \frac{\dot{m}\sqrt{(R/M)T_0}}{(\pi\, d^2/4)C_{*i}P_0} \quad , \tag{1}$$

* Certain commercial equipment, instruments, or materials are identified in this paper to foster understanding. Such identification does not imply recommendation or endorsement by the National Institute of Standards and Technology, nor does it imply that the materials or equipment identified are necessarily the best available for the purpose.

where $\dot{m}$ is the mass flow from the participant's primary flow standard, R is the universal gas constant, T_0 is the stagnation temperature, M is the molecular mass of the air, P_0 is the stagnation pressure, d is the diameter of the CFV throat, and C_{*i} is the ideal critical flow function, a property of the gas calculated from its specific heat ratio. The molecular mass was calculated based on the dew point temperature reported by the participants and dry air composition was used to calculate C_{*i} .

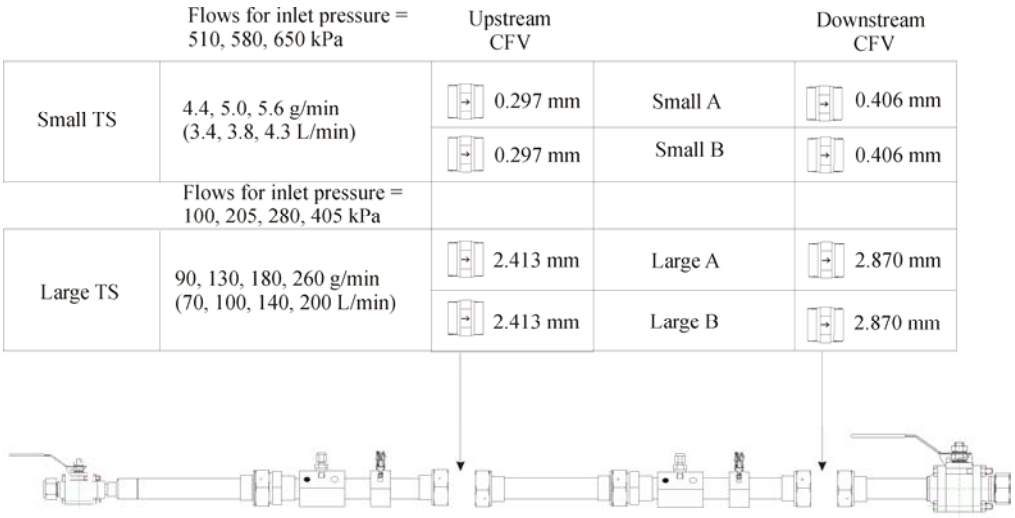

Figure 2. The transfer standard uses two CFVs in series, switched, over two flow ranges.

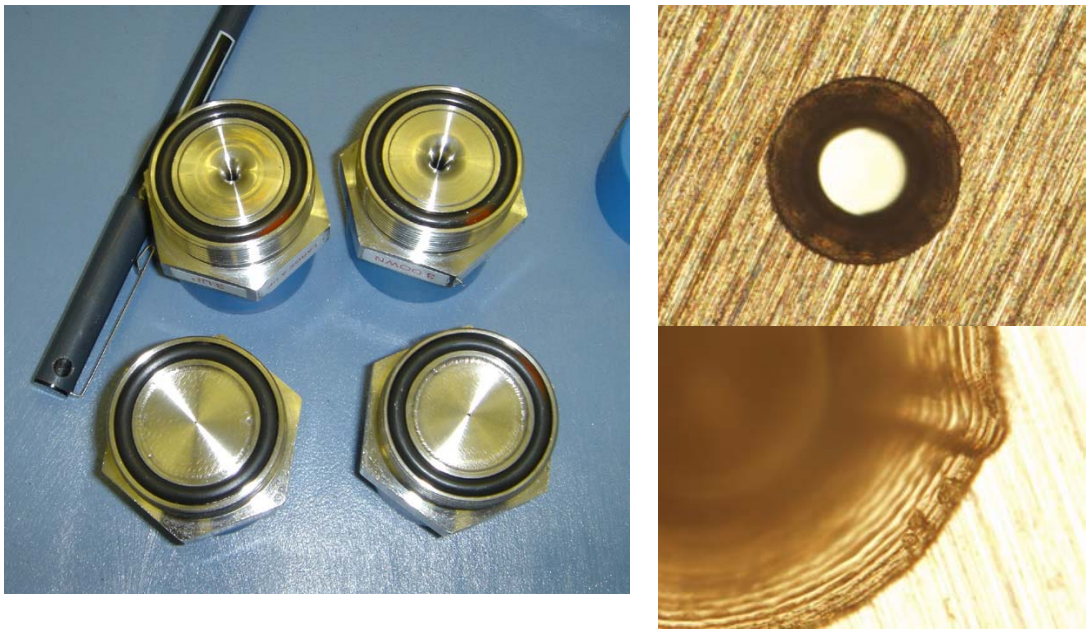

Figure 3. Four of the eight K6 critical flow venturis. Microscopic views of the 0.4064 mm (above) and 0.2794 mm (below) CFVs.

Uncertainty Analysis

The uncertainty of the discharge coefficient used to compare the participants is due to 1) the uncertainty of the mass flow measurement, 2) the standard deviation of the mean of repeated measurements in each lab, and 3) uncertainties related to the transfer standard (instrumentation, drift, environmental sensitivities, etc). In the key comparison report, the root-sum-square of all three components was used during calculation of the uncertainty of the key comparison reference value and the uncertainty of the degree of equivalence. In this paper, only the uncertainties in the last category (TS) are considered. The uncertainty of the TS was evaluated by preliminary testing done in the pilot laboratory and propagation of uncertainties analysis.

Propagation of Uncertainties

We analyzed the uncertainty contributed to the key comparison by the transfer standard following the method of propagation of uncertainties[3, 4] This involves obtaining normalized sensitivity coefficients by partial differentiation, $S_i = (x_i / C_d)(\partial C_d / \partial x_i)$. We also obtain standard uncertainties (dx_i) for the inputs to Equation 1 from evaluations of the instruments we use to measure them. The uncertainty components considered and their contribution to the uncertainty of the measurand ($S_i\, dx_i$) are listed in table 1 as a percentage of C_d. As usual, not all uncertainty components are explicitly found in the data reduction equation (in this case, temperature effects, critical flow effects, and leaks). The sources and magnitudes of uncertainty components are explained in the sections that follow.

Table 1. Uncertainty components and their magnitude (standard uncertainty or $k = 1$), for the small and large CFVs used in the K6 transfer standard.

	Uncertainty Component	**Small CFVs** (%)	**Large CFVs** (%)
1	Pressure sensors	0.013	0.013
2	Temperature sensors (1/2)	0.002	0.002
3	Critical flow function	0.008	0.008
4	Molecular mass (1/2)	0.006	0.006
5	*T* effects	0.016	0.006
6	Critical flow effects	0.006	0.006
7	Leaks	0.010	0
	Combined ($k = 1$)	0.026	0.019
	Expanded ($k = 2$)	**0.052**	**0.038**

1 Pressure Sensors

The four pressure sensors were tested for their: 1) sensitivity to room temperature changes, and 2) calibration stability during the comparison. We measured temperature sensitivity by changing the room temperature to 18.7 °C, 20.5 °C, 22.5 °C, and 24.5 °C, waiting 4 h or more between temperature changes for thermal equilibrium, and calibrating the pressure

sensors with a Ruska piston pressure gauge. The results are presented in Figure 4, shown as deviation from the correct pressure in parts in 10^6 (ppm) versus pressure.

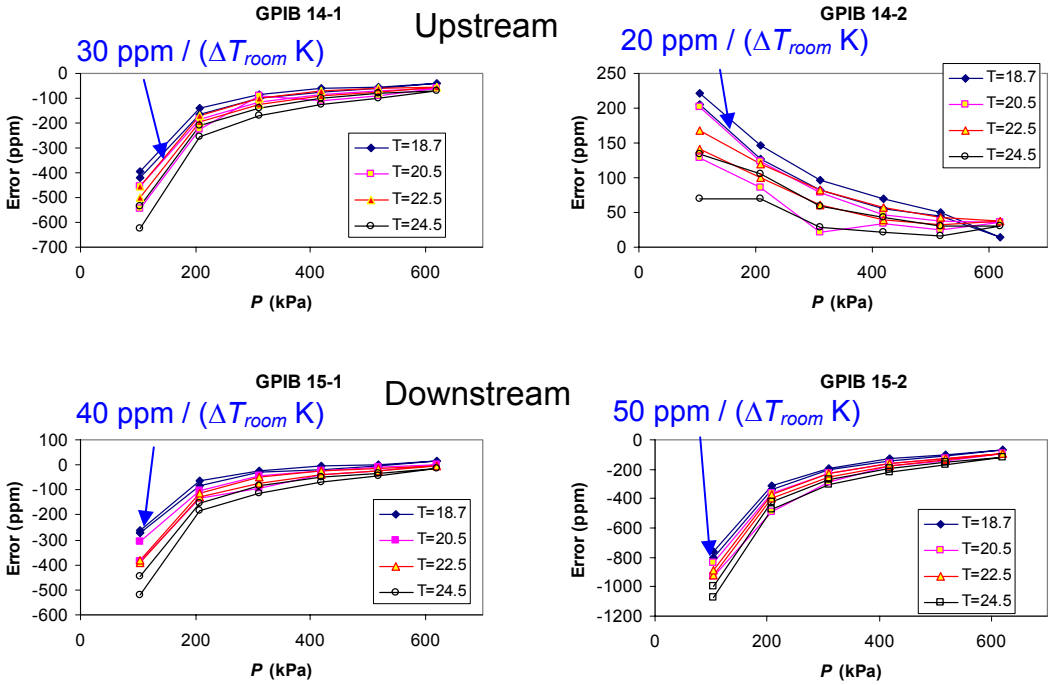

Figure 4. Temperature sensitivity for the four TS pressure sensors.

The plots in Figure 4 are labeled with the largest room temperature sensitivity, which occurs at the lowest pressure at which the sensor will be used (140 kPa and 100 kPa for the upstream and downstream sensors respectively). The largest sensitivity was 50 parts in 10^6 / (ΔT_{room} K). Based on monitoring temperature sensors included in the TS, the range of room temperatures in the participants' labs during the comparison was 19.5 °C to 25.8 °C, and for this range of temperatures we arrive at a worst case temperature effect on the pressure sensors of (6.3 K)(50 parts in 10^6 / K) = 315 parts in 10^6. We will assume that this figure covers 99 % of the temperature differences of the comparison and that they are normally distributed to arrive at a standard uncertainty of 105 parts in 10^6.

The four pressure transducers were calibrated nine times on the four occasions that the TS was at NIST during the comparison, and we found that they drifted as much as 0.05 % (see Figure 5). Corrections to the zero and gain of the sensor calibrations (as a linear function of time) were made and applied to the comparison pressure measurements. With the zero and gain corrections applied, we estimate the pressure calibration standard uncertainties (from sources other than temperature sensitivity) to be 50 parts in 10^6.

We examined the difference between redundant pressure measurements made while each lab was collecting data for the key comparison (1200 values). The standard deviation of the differences was 50 parts in 10^6.

Taking the root-sum-square of calibration drift, temperature effects on the pressure sensors, and the standard deviation of redundant pressure measurements gives the pressure uncertainty of 125 parts in 10^6 listed in table 1.

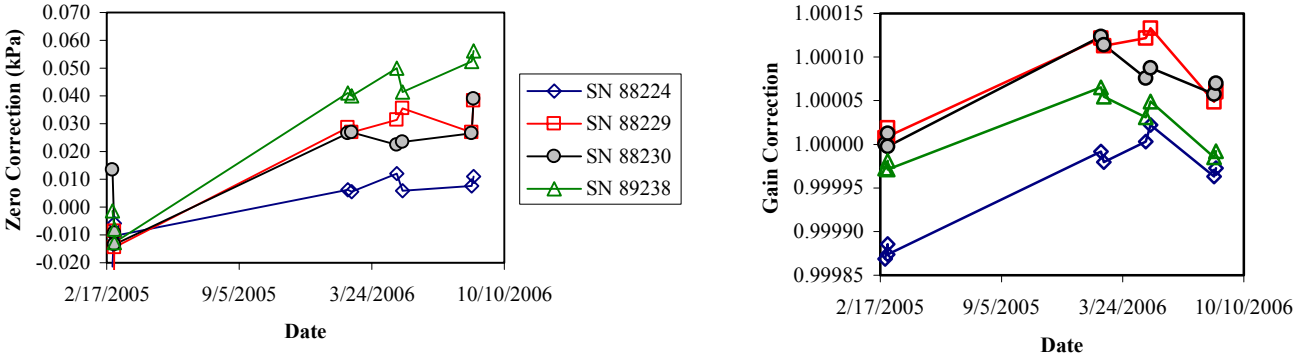

Figure 5. Drift in zero and gain for the four TS pressure sensors during the comparison.

2 Temperature Sensors

All participants used the same temperature sensors throughout the comparison so calibration biases are correlated. Calibrations performed at NIST during the comparison showed the four CFV temperature sensors to be stable within 1 mK. The temperature measurement uncertainty in table 1 also incorporates analysis of the redundant measurements made in the participants' labs (standard deviation is 40 parts in 10^6). Since temperature appears under the square root in Equation 1, its normalized sensitivity coefficient is 0.5 and 20 parts in 10^6 is listed in table 1.

3 Critical Flow Function

Errors in the value of the ideal critical flow function C_{*i} are also highly correlated for measurements between different participants. The same calculation method was used at nominally the same pressures and temperatures. However, we will not assume any uncertainty reduction due to correlation.

The C_{*i} correlation we used assumes ideal gas behavior and dry air composition:

$$C_{*i} = \sqrt{\gamma_0 \left(\frac{2}{\gamma_0 + 1} \right)^{\frac{\gamma_0 + 1}{\gamma_0 - 1}}} \quad , \qquad (2)$$

where the specific heat ratio (γ_0) was calculated from the stagnation pressure and temperature using the NIST property database called Refprop[5].

To evaluate the uncertainty of C_{*i} we have also run sample calculations of the real critical flow function, C_{*R}. To calculate C_{*R} we used thermodynamic functions for air-water mixtures from Refprop and integrated along an adiabat until we reached Mach number of unity. We examined two cases within the comparison parameter space where the

differences between C_{*i} and C_{*R} are the most extreme: 1) the case with the highest water content (T_{dp} = 280 K, $x_{H_2O} = 0.01$) and the 2) the highest pressure (645 kPa). We found that the differences between the real and ideal critical flow function values were less than 0.012 %. Applying a rectangular distribution to this difference results in a standard uncertainty of 0.012 % / $\sqrt{3}$ = 0.008 % for C_{*i}. We used C_{*i} instead of C_{*R} because of software complications in calculating C_{*R} and because the uncertainties due to using C_{*i} are acceptably small.

4 Molecular Mass

The molecular mass M of air was calculated from the dew point temperature T_{dp} provided by the participating labs. The mole fraction of water was calculated by:

$$x_{H_2O} = \frac{P_{ws}(T_{dp})}{101.325 \text{ kPa}} \quad , \tag{3}$$

where P_{ws} is the saturation water vapor pressure, calculated from T_{dp} via a best fit function.[6, 7]

The molecular mass of moist air was calculated using the formula:

$$M = (1 - x_{H_2O}) M_{Air} + x_{H_2O} M_{H_2O} , \tag{4}$$

where M_{Air} is the molecular mass of dry air[8] (28.964643 g/mol) and M_{H_2O} is the molecular mass of water (18.015 g/mol). Various references list slight difference in the composition of dry air at sea level.[9, 10, 11] We estimate that the relative standard uncertainty attributed to the variation in composition is 35×10^{-6}. The uncertainty of M_{H_2O} is negligible.

We found that for all but two of the labs, the reported values of M and those calculated from T_{dp} agreed within 0.019 %. (See Figure 6.) After conferring with these two labs, we based our values of M on the dew point temperature. We will use a standard uncertainty for the molecular mass of 0.019 % / $\sqrt{3}$ = 0.011 % and it has a normalized sensitivity of 1/2 due to the square root function in Equation 1.

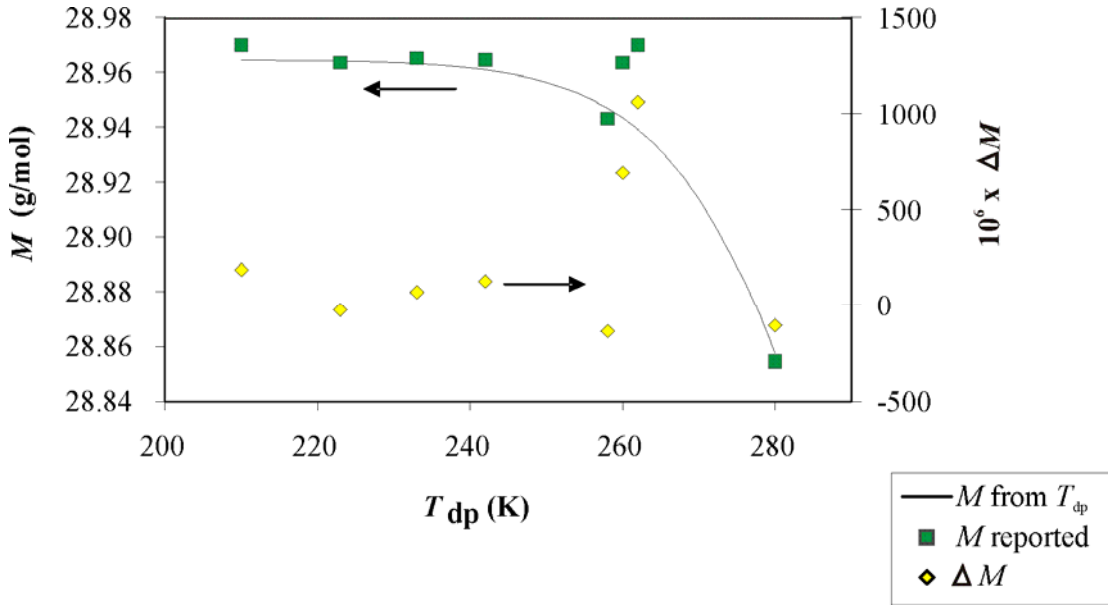

Figure 6. Molecular mass of the air used in the KC, reported and calculated from the reported dew point temperature.

5 Temperature Effects

First order temperature effects are included in Equation 1 via T_0 and C_{*i}, but second order effects cause errors that can be mistaken for lab to lab differences. The K6 CFVs were evaluated at the pilot lab for the sensitivity of the discharge coefficient to the inlet gas and room temperature. A sample data set is shown in Figure 7. In this test, the room temperature was maintained at approximately 295 K and calibration data were collected with the NIST 34 L *PVTt* standard over a range of flows. After 40 measurements, the room thermostat setting was increased to its maximum value and the temperature gradually increased to 302 K. Temperatures measured at several locations are plotted versus the number of C_d measurements made (approximately proportional to elapsed time). (See Figure 8 for explanation of the temperature nomenclature.) The change in CFV discharge coefficient from an arbitrary reference value is also plotted on the secondary Y-axis in Figure 7. The change in C_d for the 0.4064 mm CFV when the room temperature increased 7 K is 300 parts in 10^6.

The CFVs in the transfer standard are influenced by the temperature of the metered gas and by the room temperature *via* three mechanisms: 1) thermal expansion of the CFV throat area, 2) thermal boundary layer effects on mass flux at the throat, 3) temperature differences between the temperature sensor location and the CFV entrance caused by heat transfer from the room to the metered gas (sampling errors). Each mechanism is explained in the following sections.

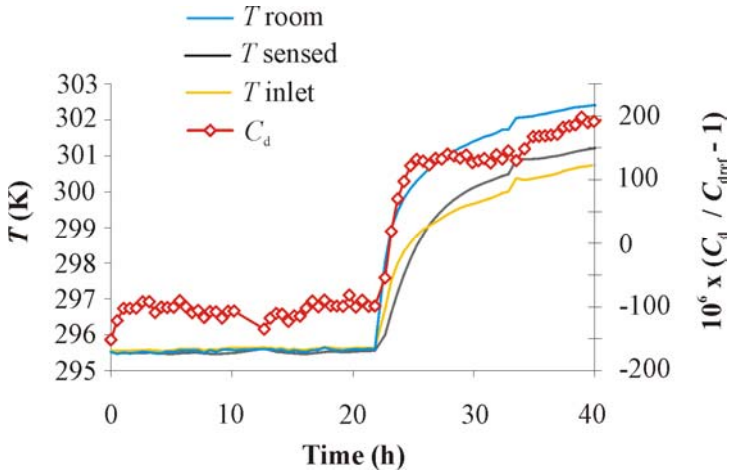

Figure 7. Effects of room temperature change on the discharge coefficient of a 0.4064 mm CFV.

Thermal Expansion: The linear thermal expansion coefficient for the CFV material (stainless steel) is 15 x 10^{-6} / K; hence, the sensitivity of the flow and discharge coefficient (through throat area) through thermal expansion is twice this value or +30 parts in 10^6 / (ΔT_{body} K).

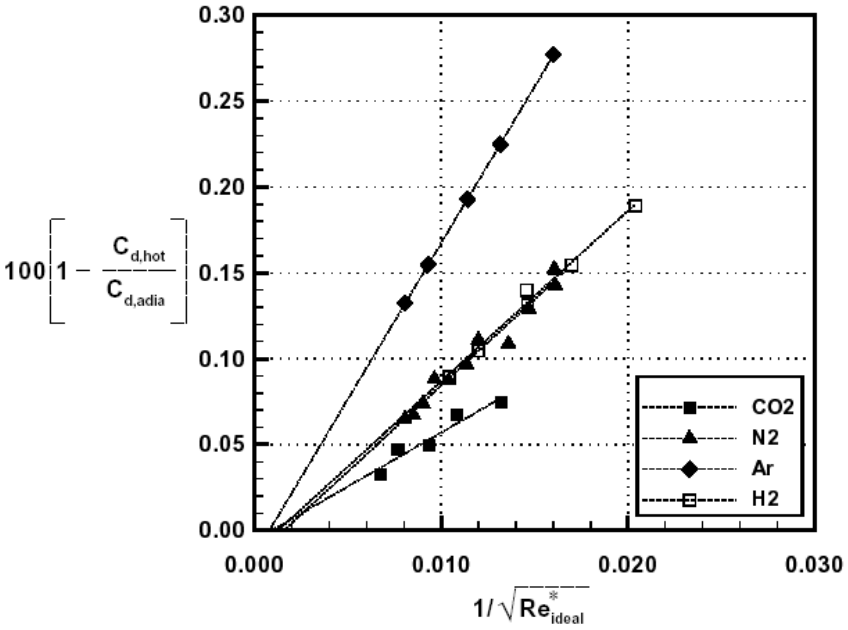

Figure 8. Percentage change in numerical discharge coefficient as a function of throat Reynolds number for an adiabatic CFV wall and a "hot" wall. (From Johnson[12])

Thermal Boundary Layer: The accepted equation for flow through a CFV (Equation 1, rearranged), assumes an adiabatic CFV wall. Actually, there is heat transfer from the CFV body to the gas flowing adjacent to the wall and this leads to a thermal boundary layer, a

layer of gas near the CFV wall that is warmer (and of lower density) than assumed in the derivation of the CFV flow equation. The thermal boundary layer leads to a lower mass flux near the wall and hence a lower discharge coefficient. Johnson[12] used numerical methods to calculate discharge coefficients for two cases: 1) the adiabatic wall and 2) the "hot" wall, i.e. a wall that has temperature equal to the gas stagnation temperature over its entire surface. The real wall temperature will fall between the adiabatic and hot wall cases, but the differences, as given in Figure 8 (reproduced from Johnson) bound the magnitude of the thermal boundary layer effects on C_d. For the 0.4064 mm nozzle ($\gamma = 1.4$ and $1/\sqrt{\mathrm{Re}} \approx 0.008$), Figure 8 predicts C_d effects of +700 parts in 10^6 or less. For the large K6 CFVs ($1/\sqrt{\mathrm{Re}} \approx 0.003$), thermal boundary layer effects predicted by Figure 8 are less than +200 parts in 10^6.

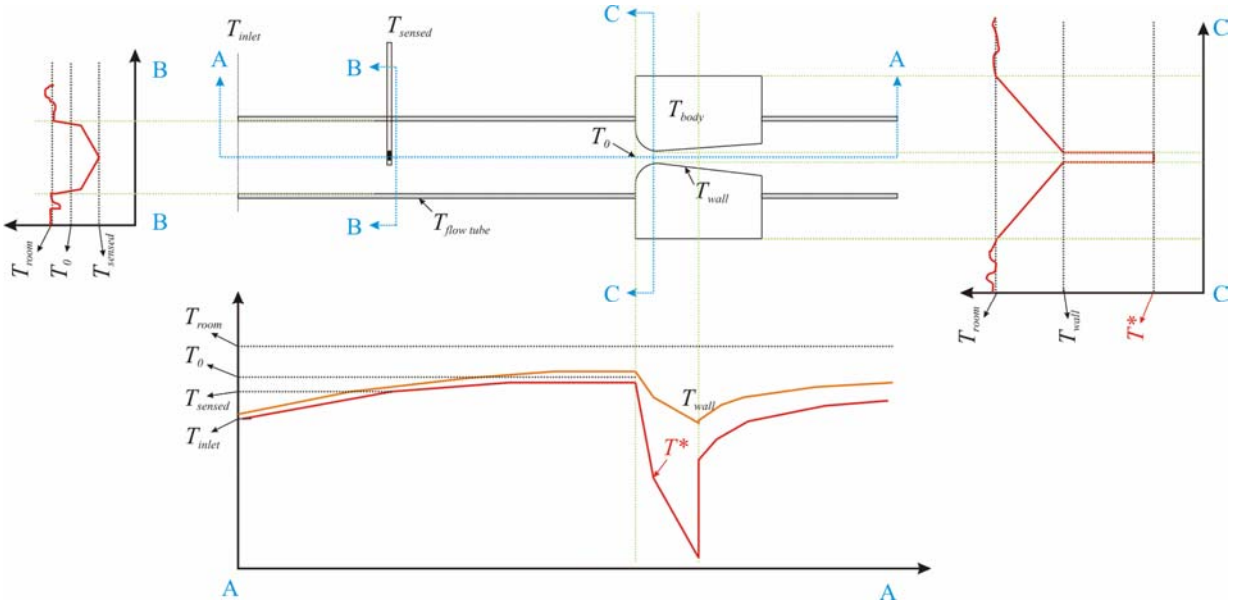

Figure 9. Temperature nomenclature and profiles illustrating temperature sampling errors.

Temperature Sampling Error: The temperature measured by a sensor in the approach pipe (T_{sensed}) may not be an accurate measure of the stagnation temperature (T_0) needed for accurate CFV mass flow calculations due to heat transfer from the room to the gas. The sensitivity of C_d to temperature sampling errors is -3400×10^{-6} /[($T_{\mathrm{sensed}} - T_{\mathrm{body}}$) K]. Figure 9 shows the predicted temperature profiles along various cross sections of the CFV and its associated piping that explain the source of sampling errors. Section B-B shows the temperature profile across the pipe at the location of the CFV temperature sensor. The gas is colder than the room because it was recently expanded through a regulator upstream (not shown). Heat transfer from the room through the pipe wall leads to radial temperature gradients at the sensor location. Two temperature profiles are shown for section A-A, one for the centerline of the pipe and CFV, the other for the wall of the pipe and CFV. The temperature gradient in the streamwise and radial directions, caused by heat transfer from the room to the cooler gas, leads to differences between T_{sensed} and T_0. It is difficult to

predict the magnitude of temperature sampling errors since they depend on many variables, including T_{inlet}, T_{room} (and their temporal and spatial variations), heat transfer coefficients (both internal and external to the pipe and CFV walls), and the geometry and thermal conductivity of the pipe and CFV materials.

To arrive at temperature bounds and associated uncertainties for the K6 comparison, the TS was tested in an environmental chamber. (See Figure 10.) Gas at nominally 295 K was fed to the TS as the chamber temperature was increased from 295 K to 305 K in approximately 2 K steps every 4 h. The 34 L and 677 L *PVTt* standards were used as the flow reference and C_d was calculated via Equation 1. The K6 pressure sensors were kept outside the environmental chamber because their temperature sensitivity was evaluated in a separate experiment and we were interested in measuring the thermal sensitivity of the CFVs alone.

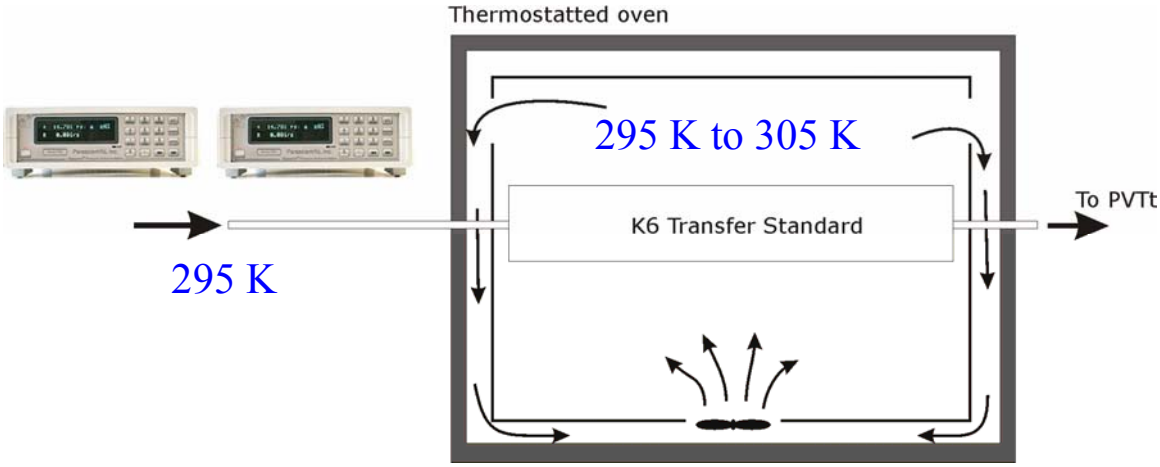

Figure 10. Test arrangement for experimental evaluation of temperature sensitivity of the K6 CFVs.

The results of the temperature sensitivity tests for CFVs from the small and large TS are shown in Figure 11. The temperature difference T_{room} - T_{sensed} is a natural choice for normalizing the temperature sensitivities since they are driven by heat transfer from the room to the gas. Both small and large CFVs use the same approach piping, and the residence time for gas there is approximately 100 times longer for the small CFV than for the large CFV. Hence, T_{sensed} for the small CFV closely follows T_{room} but there are large differences between T_{sensed} and T_{room} for the large CFV. Based on the data in Figure 11, the small CFV (0.4064 mm) shows sensitivity of $-1500 \times 10^{-6} / [(T_{room} - T_{sensed})\ \mathrm{K}]$ and the large CFV (2.87 mm) shows sensitivity of $-100 \times 10^{-6} / [(T_{room} - T_{sensed})\ \mathrm{K}]$. The larger sensitivity for the small CFV is likely due to larger thermal boundary effects and larger temperature sampling errors.

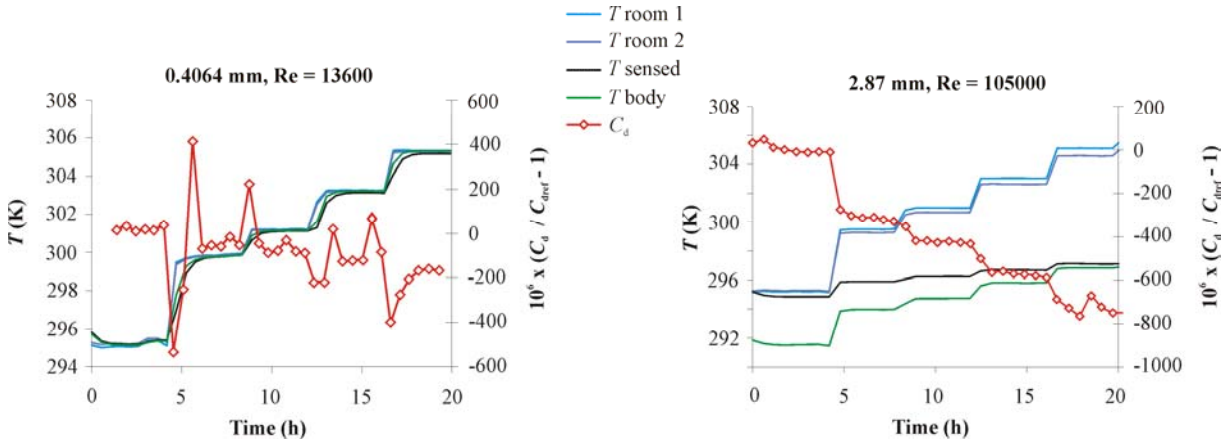

Figure 11. Experimentally measured CFV temperature sensitivity.

Based on the preliminary measurements of the temperature sensitivity, we took several steps that reduced the effects of temperature on the comparison results. We insulated the CFV body and TS piping to reduce the effect of room temperature gradients and reduce temperature sampling errors. We added a thermally conductive (aluminum) Hexcel matrix inside the flow tubes to make the gas temperature more spatially uniform. We placed two temperature bounds in the protocol: (1) 19 °C < T_{room} < 27 °C and, (2) T_{room} - T_{sensed} < 3 K.

The room temperature conditions during the comparisons ranged from 19.5 °C to 25.8 °C. The maximum difference between the room and CFV gas temperature was 1.6 K. Based on these temperature conditions and the preliminary temperature studies on the TS, the standard uncertainty due to temperature effects is 0.016 % for the small CFVs and 0.006 % for the large CFVs.

6 Critical Flow Effects

CFV theory predicts that if the pressure ratio $\left(P_{down}/P_{up}\right)$ is less than the critical value, i.e.

$$\left(P_{down}/P_{up}\right) < \left(1+\frac{\gamma-1}{2}\right)^{\gamma/(\gamma-1)}, \qquad (5)$$

changes in the downstream pressure will not cause changes in the flow through the CFV.[13] For air ($\gamma = 1.4$), the critical pressure ratio is 0.53 for the CFVs used in the TS. However, with properly designed conical diverging sections, the critical pressure ratio can be 0.75 or larger. For small CFVs (low mass flows and low Reynolds numbers), the critical pressure ratio will be much lower than 0.53. In our application of CFVs as a transfer standard, the critical pressure ratio is a concern since different participants may apply different pressures to the outlet of the TS and this will appear as lab to lab differences in the comparison. The differences in pressure can be due to different atmospheric pressure (altitude) and to pressures introduced by the participant's primary standard. For instance, a bell prover used in ascending mode uses incoming gas pressure to raise the bell from the start to stop positions.

The critical pressure ratios of the K6 CFVs were measured using the apparatus shown in Figure 12. Flow measured using CFV1 was used as a reference value. CFV1 is essentially immune from errors due to its critical pressure ratio since CFV2 largely isolates it from downstream pressure changes. The flow according to CFV2 was measured while using the 3-way valve to alternately discharge the flow to room pressure or to near vacuum. If CFV2 is operating under critical conditions, there will be negligible difference in the flow measured via CFV2 for the two discharge conditions. If it is not critical, CFV2 will indicate higher than actual flow for the higher downstream pressure.

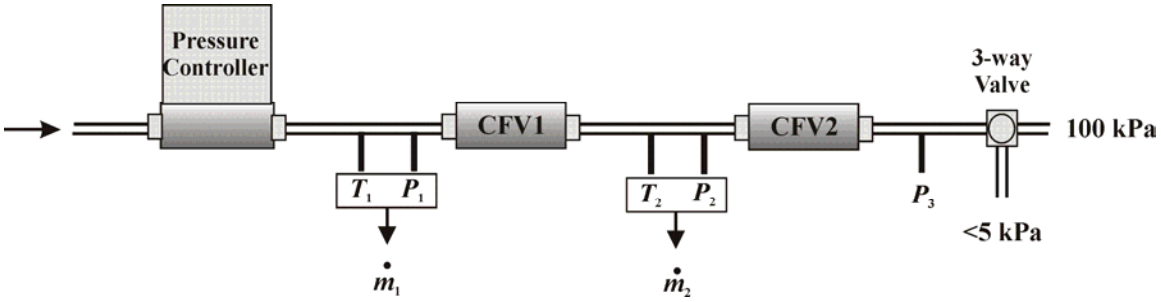

Figure 12. Apparatus used for checking the critical pressure ratio by measuring flow changes in $\dot{m}_2$ (using $\dot{m}_1$ as a reference) when the 3-way valve was used to alternately change the downstream pressure P_3 between room pressure and vacuum at.

Figure 13 presents critical pressure ratio results for the upstream (0.2794 mm) and downstream (0.4064 mm) CFVs used in the Small A and Small B TS. Based on these experiments, in order to assure discharge-condition induced uncertainties are less than 0.01 %, the small upstream CFVs should be used at pressure ratios of 0.47 or less and the downstream CFVs at pressure ratios of 0.45 or less. The actual pressure ratio for the 0.2794 mm CFVs depends on the ratio of the area of the upstream CFV to that of the downstream CFV ($0.2794^2/0.4064^2 = 0.473$). Therefore, the upstream CFVs are always used at a pressure ratio that avoids significant uncertainties. Furthermore, the downstream CFV isolates the upstream CFV from varying pressure at the outlet. The downstream CFV is of greater concern. It must be used at a pressure ratio of 0.45 or less to avoid uncertainty contributions greater than 0.01 %. The condition that the pressure at the outlet is 107 kPa or less leads to the requirements $P_2 \geq 235$ kPa and $P_1 \geq 510$ kPa. Assuming that the flow errors due to imperfect criticality are between 0 and 0.01 % (rectangular distribution with $\pm a$ =0.01 %) leads to a standard uncertainty of 0.006 %. For the Large CFVs, the pressure ratio requirements are not as severe: pressure ratios of 0.7 or less give standard uncertainty due to imperfect criticality of 0.006 %.

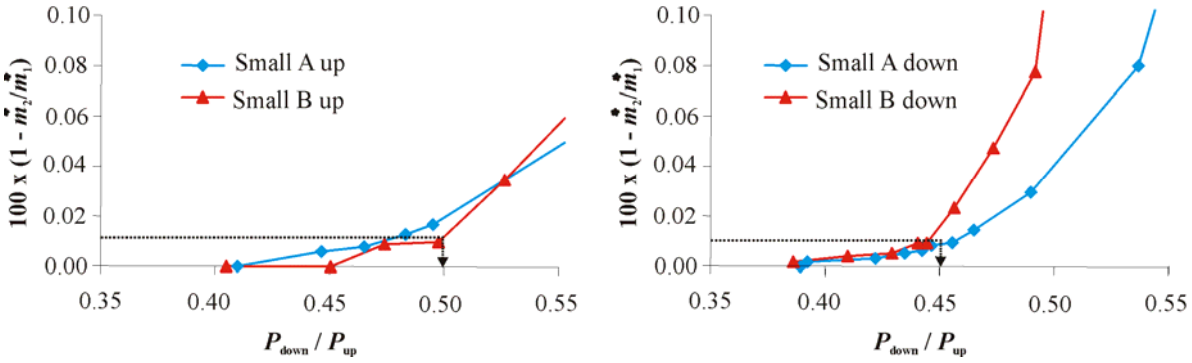

Figure 13. Change in CFV reported flow versus CFV pressure ratio for the CFVs used in the Small A and Small B transfer standard (P_2 = 220 kPa). Arrowed line indicates maximum pressure ratio to avoid errors larger than 0.01 %.

7 Leaks

A leak checking procedure was used each time the TS piping was rearranged. A program calculated the leak flow based on the rate of change of the gas density in the TS while it was pressurized and the inlet and outlet valves were closed. The leaks were less than 0.01 % of the minimum flow of the comparison. This leak is negligible for the large CFVs.

Uncertainties related to the universal gas constant and the CFV throat diameter can be ignored since the same values were used throughout the C_d calculations and they are completely correlated. Taking the root-sum-square of the components related to the TS (components 1 through 7 in table 1) gives standard uncertainties of 0.024 % and 0.018 % for the small and large TS respectively. The larger uncertainty for the small TS is due to temperature effects and leaks.

Conclusions

The transfer standard for the K6 international key comparison for low-pressure gas flow contributed a standard uncertainty of 0.026 % or less to the comparison. This figure is slightly larger than the lowest uncertainty primary standard participating in the comparison (0.025 %), but not as small as we had hoped when we began the TS design. We performed extensive preliminary testing to arrive at operating bounds and corresponding uncertainties.

The largest uncertainty components were: 1) temperature effects, 2) pressure sensors, and 3) the critical flow function. Our analysis concludes that temperature effects on CFV flow measurements can be categorized as: 1) temperature sampling errors, 2) thermal boundary layers, and 3) thermal expansion of the CFV throat. Temperature effects on small CFVs were more significant than for large CFVs. Temperature sensitivity of the pressure sensors must be considered as well. Making analytical predictions or corrections for the temperature effects on CFVs is extremely difficult, but will become necessary as primary standards improve and the expectations of transfer standards used to compare them rise.

The 0.026 % or less standard uncertainty determined by the propagation of uncertainties analysis has been supported by 1) the reproducibility of four calibrations performed at NIST during the course of the comparison (standard deviation 0.020 % and 0.009 % for the

small and large CFVs respectively), and 2) agreement between redundant flow measurements made at each lab (standard deviation 0.017 % and 0.009 % for the small and large CFVs respectively).

---

[1] Wright, J. D., *What is the "Best" Transfer Standard for Gas Flow?*, Proceedings of FLOMEKO, Groningen, Netherlands, 2003.

[2] *Measurement of Gas Flow by Means of Critical Flow Venturi Nozzles*, ISO 9300, International Organization for Standardization, Switzerland, 2005.

[3] *Guide to the Expression of Uncertainty in Measurement*, International Organization for Standardization, Switzerland, 1993.

[4] Coleman, H. W. and Steele, W. G., *Experimentation and Uncertainty Analysis for Engineers*, 2nd ed., New York, John Wiley and Sons, 1999.

[5] Lemmon, E., McLinden, M., and Huber, M., 2002, Refprop 23: Reference Fluid Thermodynamic and Transport Properties, NIST Standard Reference Database 23, Version 7.0, 7/30/02, National Institute of Standards and Technology, Boulder, Colorado.

[6] American Society of Heating, Refrigerating and Air-Conditioning Engineers, *1993 ASHRAE Handbook: Fundamentals*, Atlanta, Georgia, pp. 6.7.

[7] Hyland, R. W. and Wexler, A., *Formulations for the Thermodynamic Properties of the Saturated Phases of H_2O from 173.25 K to 473.15 K*, ASHRAE Transactions 89(2A), pp. 500 to 519, 1983.

[8] Wright, J. D., *Gas Properties Equations for the NIST Fluid Flow Group Gas Flow Measurement Calibration Services*, February, 2004.

[9] Hilsenrath, J., Beckett, C. W., Benedict, W. S., Fano, L., Hoge, H. J., Masi, J. F., Nuttall, R. L., Touloukian, Y. S., Wooley, H. W., *Tables of Thermal Properties of Gases*, U.S. Department of Commerce, NBS Circular 564, 1955.

[10] Weast, R. C., *CRC Handbook of Chemistry and Physics,* CRC Press Inc., 58th edition, Ohio, 1977.

[11] Mackenzie, F. T. and Mackenzie, J. A., *Our changing planet*. Prentice-Hall, Upper Saddle River, NJ, p 288-307, 1995 (After Warneck, 1988; Anderson, 1989; Wayne, 1991.)

[12] Johnson, A. N., *Numerical Characterization of the Discharge Coefficient in Critical Nozzles*, Ph. D. Dissertation, Pennsylvania State University, 2000.

[13] John, J. E. A., *Gas Dynamics*, 2nd ed., Prentice Hall, 1984.